BULLETIN OF THE POLISH ACADEMY OF SCIENCES
TECHNICAL SCIENCES, Vol. 66, No. 6, 2018
DOI: 10.24425/bpas.2018.125939

Design of dual flywheels with connecting rods for gamma-type Stirling engine

S. LEKCHAUM and K. LOCHAROENRAT*

Department of Physics, Faculty of Science, King Mongkut's Institute of Technology Ladkrabang, Bangkok 10520, Thailand

Abstract. A gamma-type Stirling engine, based on a dual flywheels' concept, was designed and fabricated. Optimized design of the engine, with connecting rods, was introduced to achieve a steady state of the Stirling engine cycle. Performances of the engine were therefore presented in terms of piston motion, inertia force, angular speed, pressure-volume diagram and temperature difference. It was found that optimum length of 45 mm from the connecting rod was able to reach the maximum output mechanical speed of 738 rpm at the maximum inertia force of 0.5 N. The engine offered thermal efficiency of 46.15% and total output power of 1.21 W under the temperature difference of 267 K. In the future, this design is expected to prove useful for applications in portable generators.

Key words: Stirling engine, Stirling cycle, flywheels, connecting rod.

1. Introduction

A Stirling engine is a heat engine using the principle of external combustion, relying on the temperature difference between the cold side of the power cylinder and the hot side of a displacer cylinder [1]. In general, the working fluid is air, being used for the volume compression and expansion processes according to the ideal Stirling engine cycle. Previously, a single flywheel gamma-type Stirling engine was designed and fabricated. However, the friction force in between the reciprocating parts as well as the flywheel vibration caused a mass imbalance in the entire engine system [2]. The rotational speed fluctuation is defined as a type of vibration affecting the Stirling engine crank mechanism subject to this study. This characteristic would normally result in a halt of the machine's operation [3, 4]. Many research groups have attempted continuously to boost the performance of a Stirling engine by combining it with a regenerator [5–7]. Several designs of the crankshafts have also been studied [8–11]. However, none of those designs have managed to reduce the mechanical loss. Likewise, they create an imbalance of the engine system, affecting the inertia force and angular speed.

In this contribution, the gamma-type Stirling engine is designed and constructed by means of combining the connecting rods and twin flywheels. Two flywheels behave like two cranks in order to reduce flywheel vibration and to improve the mass balance of the whole engine system. This design helps the engine reach its maximum torque. This also leads the engine to work for a longer time as compared with the single flywheel gamma-type Stirling engine. Meanwhile, the compression ratio is kept similar to the previous engine design [2]. The hot and cold sides of cylinders are made of stainless steel and brass, respectively.

Performances of the engine are therefore investigated. They include rotational speed, inertia force, temperature difference and pressure-volume diagram. Thermal efficiency and output power of the engine are also discussed. It is expected that this engine might have a high performance when it cooperates with a portable generator to create electricity.

2. Design and fabrication

Cylinder. A gamma-type Stirling engine, including two sets of cylinders and two sets of flywheels and connecting rods, was designed, as shown in Fig. 1. The displacer piston and displacer

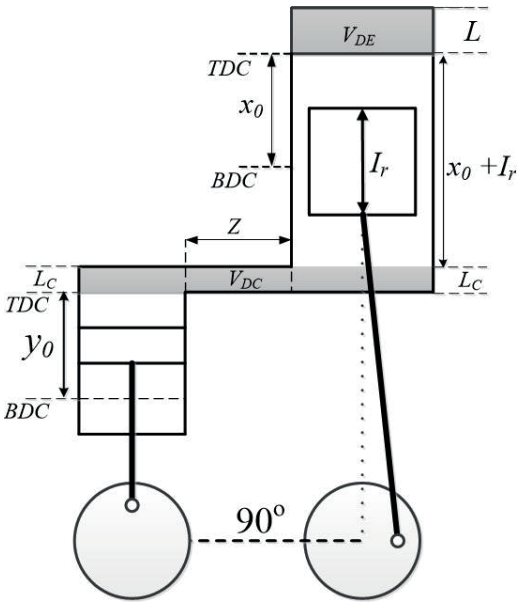

Fig. 1. Configuration of the gamma-type Stirling engine with two sets of flywheels and connecting rods

*e-mail: kitsakorn.lo@kmitl.ac.th

Manuscript submitted 2017-06-27, revised 2017-11-03 and 2018-01-12, initially accepted for publication 2018-02-01, published in December 2018.

cylinder were both center-aligned. The material descriptions are summarized in Table 1.

Table 1
Specification of the gamma-type Stirling engine

Description	Symbol	Value
Angular speed	ω_c	77.28 Hz
Area of displacer cylinder	A_{Dis}	452.38 mm^2
Area of displacer piston	A_{dis}	153.93 mm^2
Diameter of flywheel bore	a	16 mm
Diameter of crank	d	30 mm
Diameter of connecting pipe in between the cylinders	D_T	3 mm
Diameter of displacer cylinder	D_{Dis}	25 mm (brass)
Diameter of displacer piston	D_{dis}	24 mm (glass syringe)
Diameter of power cylinder	D_P	14 mm (brass)
Diameter of power piston	D'_P	14 mm (glass syringe)
Distance between hot and cold cylinders	Z	40 mm
Gap of dead volume from displacer cylinder	L	12 mm
Gap of dead volume from cold space	L_C	6 mm
Inner diameter of flywheel	D	75 mm (stainless steel)
Length of displacer piston	I_r	45 mm
Mass of flywheel	m_f	180 gm
Mass of reciprocating parts	m_p	7.60 gm
Outer diameter of flywheel	D_o	85 mm (stainless steel)
Phase angle	φ	90°
Piston stoke	x_0, y_0	20, 20 mm
Radius of crank	r_p	10 mm
Thickness of flywheel	b	8 mm

D_{Dis}, D_{dis}, x_0 and L from Table 1 were substituted in the following equations [1] to calculate:

- Swept volume of the displacer piston

$$V_{SD} = \frac{\pi D_{Dis}^2 x_0}{4}. \tag{1}$$

- Dead volume of the displacer cylinder

$$V_{DE} = \frac{\pi D_{dis}^2 L}{4}. \tag{2}$$

V_{SD} and V_{DE} were 8.83 and 5.89 cm^3, respectively, whilst the compression ratio $\beta = 1 + (V_{SD}/V_{DE})$ was 2.41. The calculated compression ratio was in agreement with theory [2]. This indicated that the engine design was to reach the best engine performance.

During the compression and expansion processes, the expansion volume of the displacer cylinder and the compression volume of the power piston as a function of the crankshaft angle (θ) were therefore calculated as follows:

- Expansion volume

$$V_E = \frac{V_{SD}}{2}(1 - \cos\theta) + V_{DE}. \tag{3}$$

- Compression volume

$$V_C = \frac{V_{SD}}{2}[1 + \cos(\theta)] + \frac{V_{SP}}{2}[1 - \cos(\theta - \varphi)] + V_{DC}. \tag{4}$$

- Swept volume of the power piston

$$V_{SP} = \frac{\pi D_{Dis}^2 y_0}{4}. \tag{5}$$

- Dead volume of compression

$$V_{DC} = \frac{1}{4}\left(\pi D_{Dis}^2 L_C + \pi D_P^2 L_C + \pi D_T^2 Z\right). \tag{6}$$

Flywheel and connecting rod. After substituting m_f, D_0 and D in the following equation [15]:

$$\text{Moment of inertia } I = \frac{m_f}{2}\left(D_0^2 - D^2\right). \tag{7}$$

the moment of inertia of the dual flywheel was $2 \times 3.61 = 7.22$ kg · mm^2. As compared with the moment of inertia of the previous single flywheel design (7.22 kg · mm^2), the present dual flywheels resulted in a reduction of the torque fluctuation and an improvement of the absorption of mechanical energy during the compression and expansion processes [10, 11]. In addition, the forced vibration could be reduced even further by combining the flywheel and the connecting rod, as shown in Fig. 2. However,

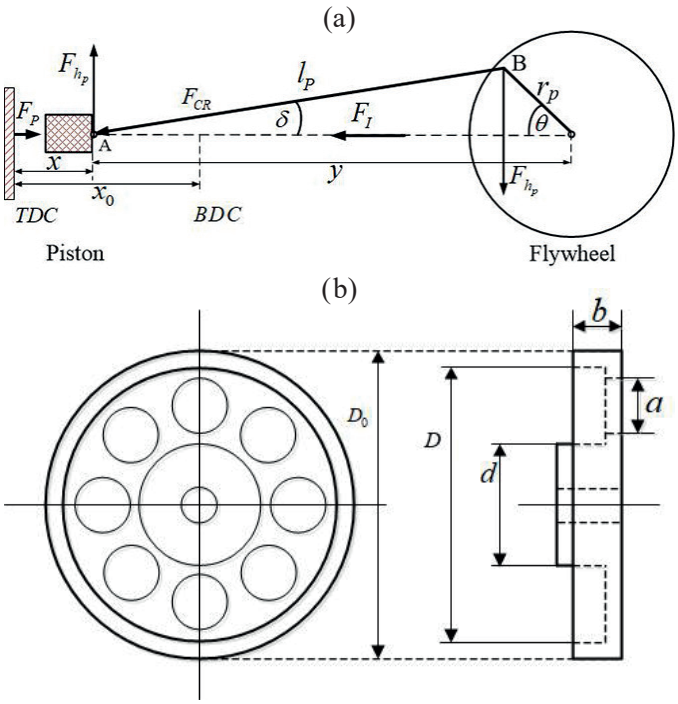

Fig. 2. Detailed design of each flywheel and connecting rod (a) and top-view and side-view of flywheel (b)

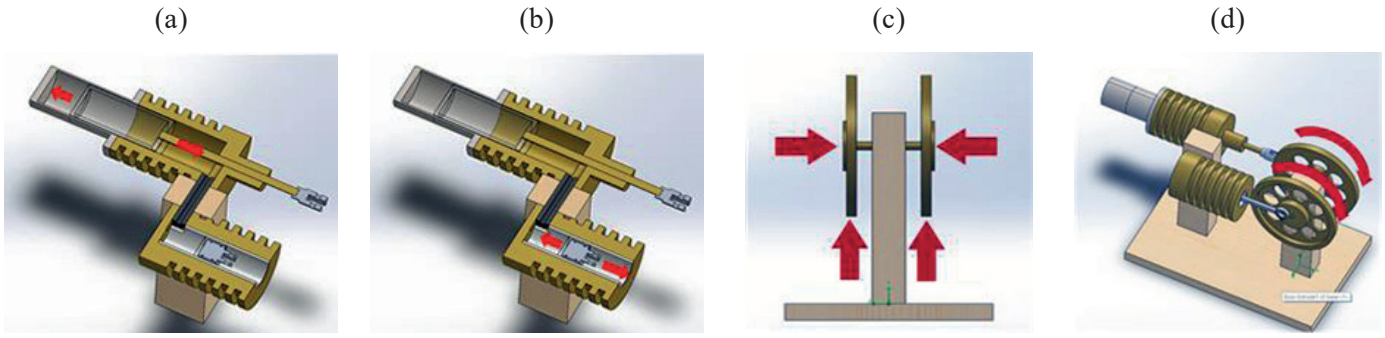

Fig. 3. Pretest model of the engine; leakage test (a), friction test (b), mass balance test (c) and assembly test (d)

optimum design of the connecting rod length was necessary for the displacer piston and power piston to move sinusoidally into an equivalent static system.

A pretest of the designed and fabricated engine was necessary to check the motion of the power piston and the mass balance of the dual flywheels according to the simplified model in Fig. 3. When the displacer piston was moved forward and backward in the closed thermodynamic system, as shown in Fig. 3a, the air pressure could force the power piston to go back and forth. It was found that the engine did not show any leakages because the power piston could go along well in between the piston's axes. The power piston was freely moved inside the displacer cylinder, as shown in Fig. 3b, meaning that the friction force was almost eliminated. The mass balance of the flywheels was satisfied, as seen in Fig. 3c, because the engine vibration disappeared. These dual flywheels had more mass balance than the single flywheel prepared as per the previous design. The time of flywheels was 15 sec. When the pistons were assembled with the flywheels, as shown in Fig. 3d, the flywheels were run continuously for 10 sec. before stopping automatically. The running time was reduced due to the effect of the weight of displacer and power pistons after connecting them with the flywheels.

Next, the engine potential in terms of mechanical and thermal performances was tested. Temperatures at the hot side (T_1 and T_2, as shown in Fig. 4) and the cold side (T_3 and T_4, as shown in Fig. 4) of the cylinders were measured with a thermometer (model: Fluke 54 II B). A Bunsen burner was used as a heat source. The flywheel's speed was detected by using the photo tachometer (model: Lutron DT-2236).

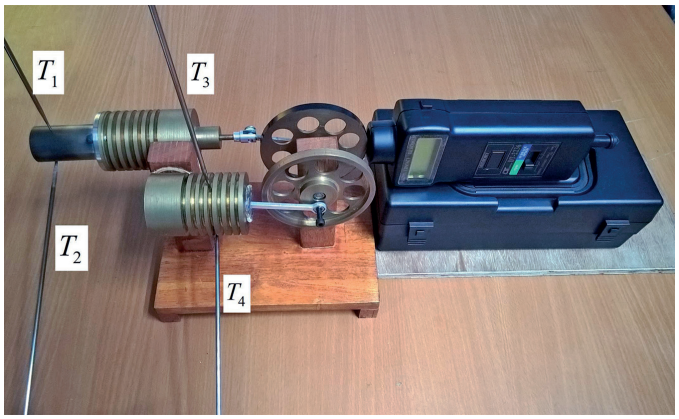

Fig. 4. Setup for testing the engine's performance

3. Results and discussion

The gamma-type Stirling engines comprising dual flywheels and connecting rods are theoretically designed based on the dynamic analysis of a slider crank mechanism and Schmidt analysis. Dynamic analysis of the slider crank mechanism under D'Alembert principle represents the limitation of the forced vibration, whereas Schmidt theory for the Stirling engine explains how the displacer and power pistons are sinusoidally working during the compression and expansion processes.

Dynamic analysis of slider crank mechanism. Under the constant stoke of 20 mm, substituting $r_p = 10$ mm and parameters l_p (i.e. 10, 15, 45 mm) in the following equation [12, 13] allows to calculate the following:
Connecting rod angle

$$\delta = \tan^{-1} \frac{r_p \sin\theta}{\sqrt{l_p^2 + r_p^2 \sin^2\theta}} \tag{8}$$

Meanwhile, the piston motions in terms of displacements x and y as a function of the crankshaft angle (θ) in Fig. 2a are calculated as follows [12, 13]:

$$x = l_P(1 + \cos\delta) + r_P(1 - \cos\theta) \tag{9}$$

$$x = l_p + r_p \cos\theta + \sqrt{l_p^2 - r_P^2 \sin^2\theta}\,. \tag{10}$$

When connecting rod length (l_p) is increased, as shown in Fig. 5, the displacement profile of x and $y - l_p$ calculated from equations (9, 10) is confirmed to be sinusoidal in form. Furthermore, the crest and trough of the sine wave are completely symmetric when the optimum length of the connecting rod is achieved or for 45 mm in this study.

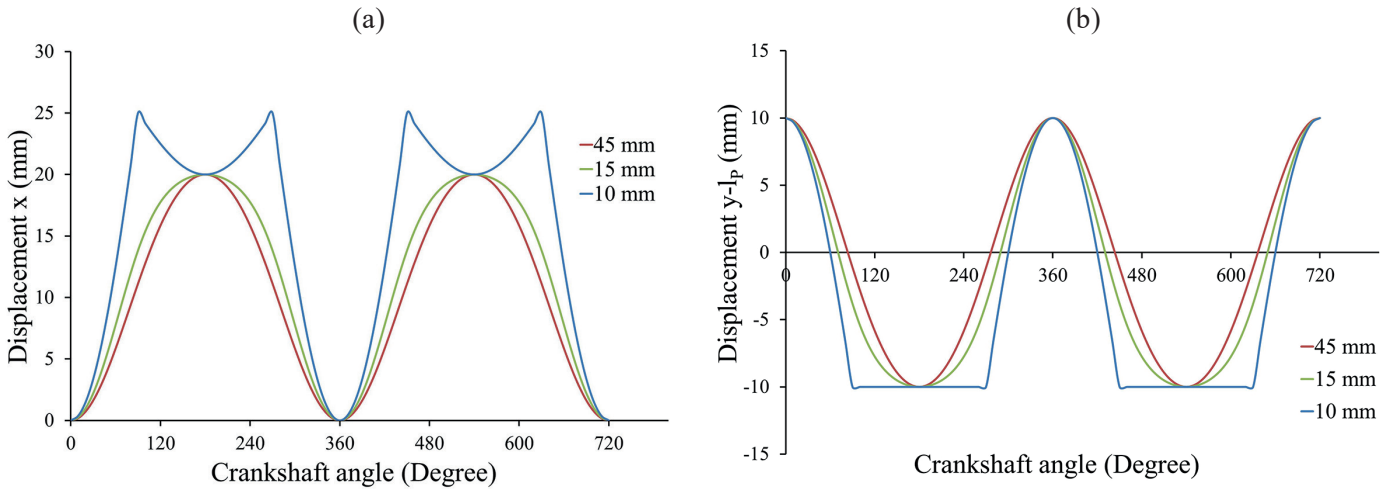

Fig. 5. Displacement x (a) and y – l_p (b) as a function of the crankshaft angle

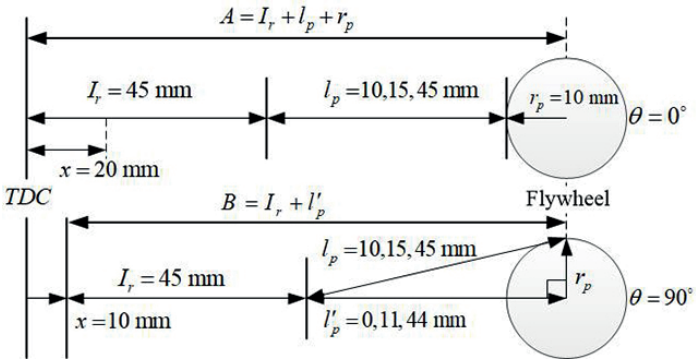

Fig. 6. Schematic diagram of displacement A and B in a one-fourth cycle with parameter l_p obtained by using a trigonometric solution

This optimum length is also confirmed by using trigonometry basics, as shown in Fig. 6. Table 2 shows that displacement A – B in a one-fourth cycle (from 0° to 90°) with only $l_p = 45$ mm conforms very well to the piston stoke of about 10 mm. Therefore, displacement A – B in half a cycle and one cycle is equivalent to the stoke design of 20 mm (Table 1).

Table 2
Displacement A – B in a one-fourth cycle together with parameters l_p

l_p (mm)	Displacement A at 0° (mm)	Displacement B at 90° (mm)	Displacement A – B (mm)
10	45 + 10 + 10 = 65	45 + 0 = 45	65 – 45 = 20
15	45 + 15 + 10 = 70	45 + 11 = 56	70 – 56 = 14
45	45 + 45 + 10 = 100	45 + 44 = 89	100 – 89 = 11

However, the engine does not work when l_p goes over 45 mm. This is a limitation of the engine that will require improvement in the future. Similarly, the engine does not work when l_p is less than 45 mm. The engine will stop working because the air pressure force is lower than the aerodynamic friction force. Substituting optimum length of the connecting rod ($l_p = 45$ mm), $r_p = 10$ m and $\theta = 90°$ in equation (8), the angle of the connecting rod is equivalent to $\delta = 12.84°$. At this angle, the displacer piston is well positioned at the center of the piston stoke while the engine is operating under a flywheel's speed (N) of 738 rpm.

According to the D'Alembert concept, the inertia force to reciprocating mass and the torque due to the inertia force are written as follows [14]:

- Inertia force

$$F_I = m_p \omega_c^2 r_P \cos\theta + \frac{m_p \omega_c^2 r_P \cos 2\theta}{l_P/r_P}. \tag{11}$$

- Torque

$$\tau = r_P F_I \left(\sin\theta + \frac{\sin 2\theta}{2\sqrt{(l_P/r_P)^2 - \sin^2\theta}} \right). \tag{12}$$

Figure 7 shows a relationship between the inertia force (equation 11) and torque (equation 12) as compared to the crankshaft angle. When the piston stoke is constantly kept at

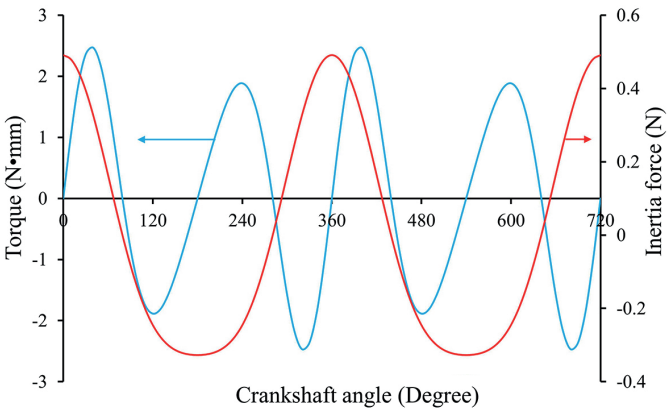

Fig. 7. Torque and inertia force as a function of the crankshaft angle

20 mm, maximum inertia force and maximum torque of the crankshaft are 0.5 N and 2.5 N · mm, respectively.

The maximum inertia force of 0.5 N offers the mass balance between the connecting rod and flywheel. Enhancement of the inertia force from the dual flywheels results in a reduction of the fluctuation of angular speed, as compared to the previous design of just a single flywheel. The current engine design is thus smoothly operated for each engine cycle under a steady state.

In addition to the inertia force, there are other three forces existing under the engine operation: the force transmitted via the connecting rod (F_{CR}), the air pressure force (F_P) and the opposite force (F_{hp}). Force transmitted via the connecting rod is related to the inertia force as follow:

$$F_{CR} = \frac{F_I}{\cos\delta}. \tag{13}$$

As a result of the maximum inertia force and maximum torque, the maximum air pressure for each engine cycle under the steady state is expressed as follows:

$$\Delta P = P_{\max} - \bar{P}. \tag{14}$$

$$F_P = \Delta P\left(\mathrm{A}_{DIS} - \mathrm{A}_{dis}\right). \tag{15}$$

After substituting the maximum air pressure $P_{max} = 142.00$ kPa and the average air pressure of displacer cylinder $\bar{P} = 101.3$ kPa in equation 14, the air pressure difference ΔP is 40.7 kPa. The maximum air pressure force (F_P) is therefore 1.57 N (Eq. 15). Considering the horizontal forces, when this air pressure force (F_P) exceeds the force transmitted via the connecting rod (F_{CR}), according to the torque supply, this much torque is applied to the two-mass system (crankshaft and power piston) in opposite direction to that of angular acceleration in order to make the system dynamically equivalent to that of the connecting rod. This is an effective design of the dual flywheels. Moreover, when the vertical forces are considered, the correction couple is introduced by two equal, parallel and opposite forces $F_{hp} = F_{CR}\sin\delta$ acting at the gudgeon pin (point A) and crank pin end (point B) perpendicular to the axis of the piston stoke, as shown in Fig. 2a. Therefore, the reaction of guides [15, 16] is firmly caused by all the forces at the power piston pin. Such minimum vibration and lateral forces acting on the piston originate from optimum design of the connecting rod length. Finally, overall performance of the Stirling engine is distinctly improved.

Schmidt analysis for Stirling engine. After the optimization design of the connecting rods and dual flywheels in the Stirling engine proves successful, the two power pistons are able to sinusoidally move perpendicular to each other under a steady state. This is confirmed by Fig. 8, indicating a relationship between the expansion and compression volumes (V_E and V_C from equations 3–4) as a function of the crankshaft angle. It is seen that the swept volume allows for heat clearance and flow passages between the hot and cold spaces conforming to the compression and expansion processes for each engine cycle. In addition, the heat power cycle indicates the different phases at 90° between the displacer cylinder and power piston.

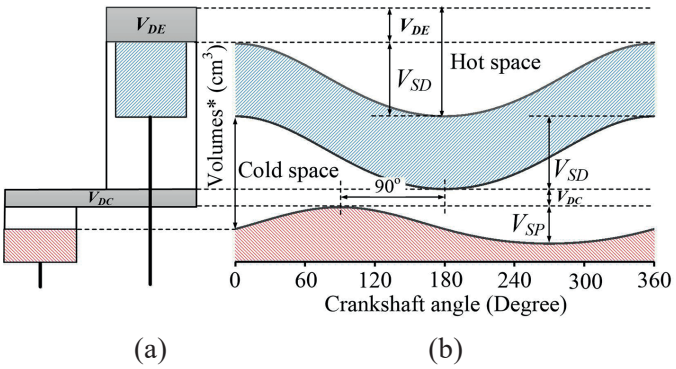

Fig. 8. Simple configuration of the gamma-type Stirling engine (a) and expansion and compression volumes as a function of the crankshaft angle (b). Volumes* at the y-axis represent the expansion and compression volumes according to equations 3–4

This compression and expansion processes are also considered reversible processes between mechanical energy and heat energy. The processes therefore proceed to produce the output mechanical power from the work generated for each engine cycle. That is, air served as the working fluid is compressed into the cold space and it is then transferred into the hot space. Hence, the compressed air is expanded and it is transferred back into the cold space. Then, net work is calculated by measuring the area under the curve from a P–V diagram, as shown in Fig. 9.

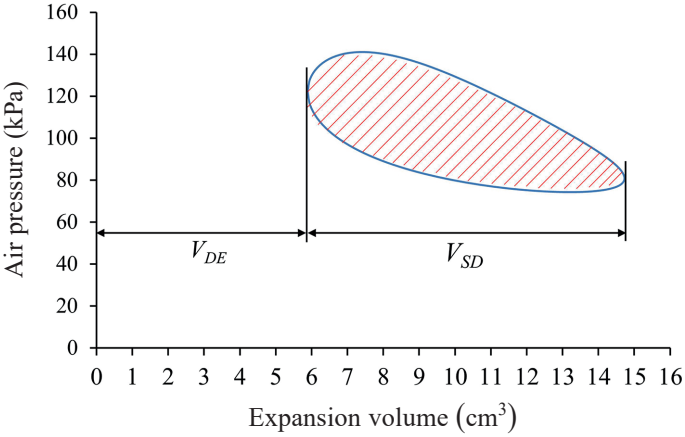

Fig. 9. Pressure-volume diagram of the engine

The expansion volume is calculated by means of equation 3, whilst the air pressure is calculated by the following equations [15]:

$$P = \frac{\bar{P}\sqrt{1-\lambda^2}}{1-\lambda\cos(\theta-\alpha)}. \tag{16}$$

where:

- Lambda

$$\lambda = \frac{\left(\gamma^2 + 2(\gamma-1)\chi_s\cos\varphi + \chi_s^2 - 2\gamma + 1\right)^{1/2}}{\gamma + 2\gamma\upsilon + \chi_s + 2\varsigma + 1}. \tag{17}$$

- Alfa

$$\alpha = \tan^{-1}\left(\frac{\chi_S \sin\varphi}{\gamma + \cos\varphi + 1}\right). \tag{18}$$

- Temperature ratio

$$\gamma = T_C/T_H. \tag{19}$$

- Swept volume ratio

$$\chi_s = V_{SP}/V_{SD}. \tag{20}$$

- Expansion volume ratio

$$\upsilon = V_{DE}/V_{SD}. \tag{21}$$

- Compression volume ratio

$$\varsigma = V_{DC}/V_{SD}. \tag{22}$$

Also, net work is indirectly calculated by the following equations:

- Net work

$$W_{net} = W_C + W_E. \tag{23}$$

- Compression work

$$W_C = \oint P dV_C = \frac{\bar{P} V_{SD} \pi \lambda \gamma \sin\alpha}{1 + \sqrt{1 - \lambda^2}}. \tag{24}$$

- Expansion work

$$W_E = \oint P dV_E = \frac{\bar{P} V_{SD} \pi \lambda \sin\alpha}{1 + \sqrt{1 - \lambda^2}}. \tag{25}$$

As a result of calculating the net work, thermal efficiency and output power of the engine, based on the Schmidt cycle, are finally calculated in the following manner [15]:

- Thermal efficiency

$$\eta = \frac{W_{net}}{W_n} \times 100\%. \tag{26}$$

- Output power

$$P = W_{net} N \tag{27}$$

where N represents a flywheel's speed. When the hot and cold sides of cylinders stand at $T_H = 574$ K and $T_C = 307$ K, respectively, the temperature difference of 267 K provides the thermal efficiency of 46.15% and the output power of 1.21 W.

4. Conclusion

A gamma-type Stirling engine was constructed based on the optimization design of the connecting rods in order to balance the dual flywheels. By varying connecting rod length from 10 to 45 mm, it was found that the engine offered its best performance under the connecting rod length of 45 mm. The engine provided thermal efficiency of 46.15% and output mechanical power of 1.21 W under the temperature difference of 267 K. In the future, this engine could be used as a source of mechanical power for small portable generators.

Acknowledgements. This work was supported by King Mongkut's Institute of Technology Ladkrabang, Bangkok 10520, Thailand. The authors would also like to thank Khaneungchat Saenyot for his helpful assistance.

References

[1] G. Walker, *Stirling Engine*, Clarendon Oxford, UK, 1980.
[2] K. Seanyot, K. Locharoenrat, and S. Lekchaum, "Design and fabrication of Gamma-type Stirling engine on parabolic dish of solar concentrator by a compression ratio method", *Applied Mechanics Materials* 851, 383–388 (2016).
[3] A.J. Martyr and M.A. Plint, *Engine Testing Theory and Practice*, 3rd Ed., Elsevier, USA, 2007.
[4] R.G. Budynas and J.K. Nisbett, *Mechanical Engineering Design*, 10th Ed., McGraw-Hill, USA, 2005.
[5] P. Puech and V. Tishkova, "Thermodynamic analysis of a Stirling engine including regenerator dead volume", *Renewable Energy* 36, 872–878 (2011).
[6] R. Gheith, F. Aloui, and S.B. Nasrallah, "Study of the regenerator constituting material influence on a gamma type Stirling engine", *Journal of Mechanical Science and Technology* 26(4), 1251–1255, (2012).
[7] R. Li, L. Grosu, and D. Queiros-Condé, "Losses effect on the performance of a Gamma type Stirling engine", *Energy Conversion and Management* 114, 28–37 (2016).
[8] B. Kongtragool and S. Wongwises, "Thermodynamic analysis of a Stirling engine including dead volumes of hot space, cold space and regenerator", *Renewable Energy* 31(3), 345–359 (2006).
[9] R. Beltran-Chacon, D. Leal-Chavez, D. Sauceda, M. Pellegrini-Cervantes, and M. Borunda, "Design and analysis of a dead volume control for a solar Stirling engine with induction generator", *Energy* 93, 2593–2603 (2015).
[10] H. Karabulut,"Dynamic analysis of a free piston stirling engine working with closed and open thermodynamic cycles", *Renewable Energy* 36(6), 1704–1709 (2011).
[11] F. Formosa and G. Despesse, "Analytical model for Stirling cycle machine design", *Energy Conversion Management* 51(10), 1855–1863 (2010).
[12] R.S. Khurmia and J.K. Gupta, *Machine Design*, Eurasia Publishing House, USA, 2005.
[13] M.J. Rider, *Design, and Analysis of Mechanisms: A Planar Approach*, Wiley, USA, 2015.
[14] S.A. Frank, "D'Alembert's direct and inertial forces acting on populations: The price equation and the fundamental theorem of natural selection", *Entropy* 17, 7087–7100 (2015).
[15] G. Schmidt, "The theory of Lehman's calorimetric machine", *Vereines Deutcher Ingenieure* 15(1), 15–20 (1871).